Soft Matter

PAPER

View Article Online
View Journal | View Issue

Cite this: *Soft Matter*, 2017, 13, 6439

Use of RAFT macro-surfmers for the synthesis of transparent aqueous colloids with tunable interactions†

Umberto Capasso Palmiero,*[a] Azzurra Agostini,[a] Enrico Lattuada,[a] Simone Gatti,[a] Jaspreet Singh,[a] Christopher Thomas Canova,[b] Stefano Buzzaccaro*[a] and Davide Moscatelli[a]

Received 31st May 2017,
Accepted 30th August 2017

DOI: 10.1039/c7sm01084b

rsc.li/soft-matter-journal

We propose a new method to produce fluorinated nanoparticles (NPs) based on *ab initio* reversible addition–fragmentation chain transfer (RAFT) emulsion polymerization without the use of toxic surfactants. NP size, surface charge, and chemistry can be controlled *via* the adoption of different macromolecular transfer agents produced *via* RAFT polymerization of amphiphilic monomers. Thanks to this versatility, interparticle interactions can be easily tuned by changing solvent composition and temperature. In addition, the refractive index and density of the solvent can simultaneously match those of the NPs by adding sodium polytungstate, an organic salt widely used for density gradient centrifugation. These colloids may be used as model systems for the study of self-assembly and aggregation in aqueous media when optical methods are required.

Fluorinated polymeric nanoparticles (NPs) have gained much attention due to their unique properties, like high hydrophobicity and lipophobicity, chemical stability, biological compatibility, low refractive index, and high gas permeability.[1,2]

More recently they have found several applications in medicine such as drug delivery systems (*e.g.* for PTX,[3] proteins,[4] and O_2 delivery[5]). These carriers are particularly useful to formulate fluorinated therapeutics like some anesthetics, which have little or no solubility in both water and oil phases (*e.g.* sevofluorane[6,7]). Their adoption as a probe in ^{19}F magnetic resonance imaging (MRI) is another emerging biomedical application and it is mainly related to their ability to act as carriers with high payload of imaging agent, biocompatibility, longer circulating half-life, and selectivity to the site of interest.[8–10]

In addition, colloidal dispersions are a common model system used to investigate fundamental physics in condensed matter. Since the fundamental work by Pusey and van Megen,[11] sterically stabilized poly(methyl methachrylate) (PMMA) particles suspended in non-aqueous solvents are widely employed to mimic the behavior of a hard sphere system. On the other end, an equivalent model system for water-based suspensions is not readily available. In fact, these studies require, in general, the use of optical techniques such as confocal microscopy and light scattering, with the need of transparent samples. For this reason, the refractive index of the particles should be very close to that of the solvent to avoid multiple scattering effects. Nevertheless, matching of the refractive index of the NPs with the solvent can rarely be obtained when water is the dispersion medium, due to its low refractive index compared to most common polymers. In the last years, taking advantage of their relatively low refractive index, fluorinated NPs were proposed as model systems to study interconnection between rheological behavior, dispersion microstructures, interparticle interactions and particle dynamics in aqueous solvent. In literature there exists a limited number of experiments where perfluorinated NPs have been used,[12–14] but in these cases the synthesis protocol requires complex and dangerous fluorine chemistry.

The use of partially fluorinated methacrylates in the synthesis of these NPs has several advantages such as (i) higher solubility in common organic solvents compared to the perfluorinated monomers, (ii) similar reactivity with the completely hydrogenated methacrylates, and (iii) the possibility to synthesize block-copolymers that can self-assemble in water. According to the literature, one of the most effective methods to synthesize this kind of nanodispersions is emulsion polymerization,[15] but the

[a] *Department of Chemistry, Material Science, and Chemical Engineering "Giulio Natta", Politecnico di Milano, 20133 Milano, Italy. E-mail: umberto.capasso@polimi.it, stefano.buzzaccaro@polimi.it*
[b] *Department of Chemical Engineering, Massachusetts Institute of Technology, Cambridge, MA 02139, USA*

† Electronic supplementary information (ESI) available: NMR analysis of the RAFT macro-surfmers, GPC snd NMR analysis of the PEGylated block-copolymer that forms the neutral fluorinated NPs, Np size distributions, recap table of the NPs synthesized and description of the optical setup for fluorescent microscopy and DDM. GelFluo.avi: a live video of the evolution of a fluorescent NPs gel upon temperature variation (see Fig. 10). See DOI: 10.1039/c7sm01084b

serious drawback of this process is the need of a surfactant which is often a toxic compound.[16,17] The concern is even higher when fluorinated surfactants are used in the emulsion polymerization of perfluorinated or partially fluorinated monomers.[18,19]

In general, fluorinated nanodispersions have poor colloidal stability due to the fact that they are hydrophobic and lipophobic at the same time. Moreover, common hydrogenated surfactants are usually not able to stabilize them because of the low compatibility between the compounds: the weak molecular interaction of the fluorinated compounds leads to the formation of a third fluorinated phase separated from the lipophilic and the hydrophilic one. For this reason, fluorinated surfactants are often required.[20]

This problem can be overcome in the emulsion polymerization by substituting the surfactant with a surface active species bearing a double bond that can be covalently incorporated into the latex.[21] Nevertheless, the use of these polymerizable surfactants with a highly hydrophobic and low reactive monomer, as fluorinated methacrylates, may lead to charge burial and colloidal instability, followed by NP aggregation.[22–24] This phenomenon is caused by the fast incorporation of the surfmer into the polymer matrix and limits the control over the final latex concentration and NP size (D_n).

Different approaches have been recently proposed to synthesize partially fluorinated methacrylate particles, usually stabilized by PEG.[25–27] While they are able to produce monodisperse suspensions, they present many disadvantages such as low conversion, unwanted secondary reactions, poor control in the final NP sizes, and complex multi-step reactions synthesis protocols.

To avoid the aforementioned problems of charge burial and use of a free surfactant, the novel process of *ab initio* reversible addition chain transfer (RAFT) emulsion polymerization has been proposed.[28] The RAFT process is a living polymerization that allows the control over the molecular weight by adding a thio-compound as chain transfer agent.[29] The first attempts to transfer the living character of this process into heterogeneous phase led to poor molecular weight control, broad molecular weight distribution and phase separation.[30] Most of the RAFT agents are fairly water-insoluble, making their transportation process from the monomer droplets to the micelles very slow and prone to variability, while the use of more water soluble RAFT agents can show significant inhibition or retardation, probably due to the interference with the process of radical entry into particles during the emulsion polymerization.

This problem has solved adopting a surface active RAFT agent able to self-assemble into micelles,[28] allowing one (i) to work with a surfactant-free process, (ii) to directly locate the living agent into the micelles without any difficulties in the diffusion phenomena, (iii) to control the molecular weight by further growing of the surface active species, (iv) to directly produce well-defined block-copolymers in water, (v) to functionalize the NP surface, and (vi) to control particle morphology. These macromolecular chain transfer agents are usually produced by a sequential RAFT polymerization of a hydrophilic monomer (*e.g.* acrylic acid) followed by a hydrophobic one (*e.g.* butyl acrylate, methyl acrylate) in the presence of a water insoluble RAFT agent.[28]

The first reported use of a fluorine-containing amphiphilic RAFT agent in the emulsion polymerization of a fluorinated monomer is that of a block-copolymer of polyacrylic acid and polyhexafluorobutyl acrylate,[31] employed in the *ab initio* RAFT emulsion polymerization of hexafluorobutyl acrylate. In this case, the hydrophobic and hydrophilic blocks are prepared in two different steps to obtain a species that acts as a surfactant and grows during the RAFT emulsion polymerization.

In the present work, an alternative way to produce surfactant-free fluorinated NPs has been assessed through the adoption of the so-called RAFT-macro surfmers, chain transfer agents that are directly synthesized *via* the RAFT polymerization of surfmers. As long as they preserve their amphiphilic behavior, they do not require a fluorinated and/or lipophilic block to be used as polymeric surfactant in the RAFT emulsion polymerization.

In order to show the flexibility of this method in terms of NP composition, dimension, and surface charge, three different kinds of surfmers were synthesized. These species have been used in the RAFT emulsion polymerization of a partially fluorinated monomer, 1,1,1,3,3,3-hexafluoroisopropyl methacrylate (HFIPM), mitigating both the charge burial and the fast incorporation of the surfmers they derived from and allowing the production of NPs with a high colloidal stability. Due to this process, it was possible to produce fluorinated NPs with good characteristics in terms of polydispersity and a wide size range (from less than 70 nm up to 386 nm) and surface charge (ζ-potential from −60 mV to +25 mV).

In the second part of the paper we show the use of our NPs as a model system to study gelation. In the first example we take advantage of the great stability of our charged NPs due to the synergy of electrostatic and steric stabilization. In the second case we exploit the capability of controlling the hydrophilicity of PEG-surfmers to create thermo-reversible gels.

1 Experimental section

1.1 Materials

Poly(ethylene glycol)methyl ether methacrylate (PEGMA950, M_n 950 Da, Sigma Aldrich), poly(ethylene glycol)methyl ether methacrylate (PEGMA2000, M_n 2000 Da, 50 wt% in water, Sigma Aldrich), [2-(methacryloyloxy)ethyl] trimethylammonium chloride (MADQUAT, 80 wt% in water, Sigma Aldrich), 3-sulfopropyl methacrylate potassium salt (SPMAK, 98%, Sigma Aldrich), 4-4′ azobis(cyanovaleric acid) (ACVA, 98%, Sigma Aldrich), 4-cyano-4-(phenylcarbonothioylthio)-pentanoic acid (CPA, >97%, Sigma Aldrich), 1,1,1,3,3,3-hexafluoroisopropyl methacrylate (HFIPM, Apollon Scientific), 2,2′-azobis(2-methylpropionitrile) (AIBN, 98%, Sigma Aldrich), were used as received except when specifically noted. 2,2′-Thiodiethanol (TDE) and Sodium Polytungstate (SPT) were purchased from Sigma Aldrich and used as they are. All the analytical-grade solvents used were purchased from Sigma Aldrich.

1.2 Synthesis of RAFT macro-surfmers

The synthesis of neutral, negatively and positively charged RAFT macro-surfmer was carried out in the presence of the CPA as RAFT agent.

1.2.1 PEGylated RAFT macro-surfmers. The production of two different PEGylated RAFT macro-surfmers was carried out using PEGMA950 to CPA molar ratio equal to 10 and PEGMA2000 to CPA molar ratio equal to 5 in order to obtain $(PEGMA950)_{10}$ and $(PEGMA2000)_5$ macro-CTAs, respectively. As an example, for the synthesis of $(PEGMA950)_{10}$, 3.94 g (2.08×10^{-1} mol L^{-1}) of PEGMA950, 113 mg (2.03×10^{-2} mol L^{-1}) of CPA and 37 mg (6.76×10^{-3} mol L^{-1}) of ACVA were dissolved in 20 mL of ethanol. The solution was poured in a septum-sealed flask, purged for 5 minutes with nitrogen and heated to 65 °C in a constant temperature oil bath under magnetic stirring for 20 h. After drying under air, the polymer was washed three times using diethyl ether and then centrifuged. PEGMA950/2000 conversion, M_n and dispersity ($Đ$) were determined by gel permeation chromatography (GPC) with a Jasco LC-2000Plus apparatus. Samples were analyzed in THF at a concentration of 4 mg mL^{-1} after filtration through a 0.45 μm pore-size membrane. The separation was performed at a flow rate of 0.5 mL min^{-1} and at 35 °C with three Superchrom PLgel 5 μm columns (600 × 7.5 mm, measuring range 0.5–1000 kDa). Molecular weights were determined from differential refractive data and were relative to poly(styrene) standards.

1.2.2 Negatively charged RAFT macro-surfmer. 0.51 g of SPMAK, 57 mg of CPA and 18 mg of ACVA were dissolved in 3.63 g of a mixture of ethanol (70 wt%) and acetic buffer (pH = 5.2, 0.27 mol L^{-1} acetic acid and 0.73 mol L^{-1} of sodium acetate). The solution was poured in a septum-sealed flask, purged for 5 minutes with nitrogen and heated to 65 °C in a constant temperature oil bath under magnetic stirring for 20 h. The polymer was purified by dialysis with a 3.5 kDa MWCO membrane tubing (SpectraPor). SPMAK conversion was determined by ^{1}H-NMR in D_2O. The choice of the ethanol/acetic buffer mixture is related to the insolubility of the SPMAK in pure ethanol and the insolubility of CPA in water. The acetic buffer at pH 5.2 was used to avoid the hydrolysis of the RAFT agent.

1.2.3 Positively charged RAFT macro-surfmer. Three different positively charged RAFT macro-surfmers were produced by varying the MADQUAT to CPA and PEGMA950 to CPA molar ratio. We obtain an homopolymer made up of 10 MADQUAT units $((MADQUAT)_{10})(MADQUAT)_{10}(PEGMA950)_{10}$ and two copolymers, one made up of 5 MADQUAT and 10 PEGMA950 units $((MADQUAT)_5(PEGMA950)_{10})$ and the other one made up of 10 MADQUAT and 10 PEGMA950 units $((MADQUAT)_{10}(PEGMA950)_{10})$. As an example, for the latter RAFT macro-surfmer, 0.5 g of MADQUAT, 2.28 g of PEGMA950, 67 mg of CPA and 20 mg of ACVA were dissolved in 17.78 g of a mixture of ethanol (70 wt%) and acetic buffer. The solution was poured in a septum-sealed flask, purged for 5 minutes with nitrogen and heated to 65 °C in an oil bath under magnetic stirring for 20 h. The polymer was purified by dialysis with a 3.5 kDa MWCO membrane tubing (SpectraPor). The conversion of the positively RAFT macro-surfmers was determined by ^{1}H-NMR in D_2O.

1.3 Synthesis and scale-up of fluorinated nanoparticles

The *ab initio* RAFT emulsion polymerization was carried out at different RAFT macro-surfmers to HFIPM weight ratios and at several monomer concentrations in order to produce NPs with different size and surface charge. In a typical experiment, 0.03 g of RAFT macro-surfmer, 7 mg of ACVA were dissolved in 3 mL of acetic buffer and poured in a 4 mL vial. 0.15 g of HFIPM was added and the sealed vial was immersed in a constant temperature oil bath at 65 °C and at a stirring speed of 400 rpm. After 24 h, the conversion of the samples was measured gravimetrically and it was found always lower than 60%, thus 7 mg of AIBN was added and the reaction mixture was left in the oil bath for other 24 h, in order to raise the conversion of the low reactive fluorinated HFIPM monomer.

The scale up of the NPs was performed in a 50 mL round bottom flask under vigorous stirring for two particular types of NPs, the ones stabilized with $(PEG2000)_5$ and the other ones with $(SPMAK)_{10}$. In addition, Rhodamine – a fluorescent dye – was covalently attached to the NPs *via* the adoption of a Rhodamine methacrylate. The synthesis of this latter species is already reported in literature.[32] Briefly, Rhodamine B (50 mg, 0.104 mmol), HEMA (135 mg, 1.04 mmol) and DCC (43 mg, 0.208 mmol) were dissolved in 63.5 g of DCM and stirred overnight at room temperature. The reaction mixture was then stored in the fridge. For the synthesis of the negative fluorescent nanoparticles, 2.5 g of $(SPMAK)_{10}$ and 143 mg of ACVA were dissolved in 45 g of acetic buffer. 2.5 g of HFIPM was then added, the mixture purged with nitrogen for 10 minutes and heated to 65 °C under stirring for 24 h. 2.5 g of the HEMA-RhB solution was evaporated and dissolved in 2.5 mL of ethanol. This solution was added dropwise in the first hour of the polymerization. After 24 h, 143 mg of AIBN was added to improve the conversion of the NPs. The scaled up PEGylated NPs were synthesized in a similar manner. Briefly, 1.43 g of $(PEG2000)_5$ and 81 mg of ACVA were dissolved in 45 g of acetic buffer. 3.57 g of HFIPM was then added. The mixture was then purged with nitrogen for 10 minutes and heated to 65 °C under stirring for 24 h. After 24 h, 81 mg of AIBN was added to improve the conversion of the monomer. An aliquot of scaled-up PEGylated NPs was dried under air, dissolved in hexafluoroisopropanol (HFIP) with 0.02 M K-TFAc and analyzed *via* an Agilent 1100 GPC/SEC unit equipped with two PFG linear M columns (PSS) connected in series with an Agilent 1100 VWD/UV detector operated at 230 nm. Sample was eluted at 1 mL min^{-1} at room temperature. Another aliquot of the same NPs was dried under air, dissolved in HFIP-d2 and analyzed *via* ^{1}H-NMR.

1.4 Methods

1.4.1 TEM and SEM analysis. Transmission electron microscopy (TEM) was carried out using a Philips CM200 electron microscope at 200 kV, equipped with a Field Emission Gun filament. The NPs were dropped onto a 200 mesh carbon-coated copper grid and dried before analysis. A Gatan US 1000 CCD camera was used and 2048 × 2048 pixels images with 256 grey levels were recorded. Scanning electron microscope (SEM) was

performed on a Zeiss Leo 1530 operated at an accelerating voltage of 3 kV. The latex was coated in a Safematic CCU-010 HV using a Pt–Pd (80–20) target, whereas the layer thickness was set at 4 nm.

1.4.2 Dynamic laser light scattering (DLLS). NP size, polydispersity index (PDI), and ζ-potential were determined by DLLS (Zetasizer Nano Series, Malvern Instruments). Some representative samples were analyzed using a custom made, variable-angle, DLLS setup, equipped with a fast digital correlator to obtain the full intensity correlation function and better determine the PDI.

The light scattering apparatus includes a frequency-doubled Nd:Yag laser operating at $\lambda = 532$ nm, a temperature controlled cell (precision 0.01 °C), a photomultiplier tube mounted on a rotating arm, and a digital correlator. The incident laser beam is vertically polarized. The detected polarization is selected by a Glan–Thompson prism, and the scattered intensities polarized perpendicular and parallel to the horizontal scattering plane are measured at 90 degrees.

The hydrodynamic radius and PDI were extracted from a third-order cumulant analysis. The first cumulant describes the average decay rate of the distribution. The second and the third cumulants directly correspond to the appropriate moments about the mean, the second moment being related to the variance, and the third moment providing a measure of the skewness – or asymmetry – of the distribution.

1.4.3 Refractive index. The refractive index of solvents was measured with an Abbemat MW digital refractometer at 589.3 nm Na-D wavelength.

To determine the refractive index of the NPs we exploited the dependence of the intensity of the scattered light on the mismatch between the particle and the solvent refractive index. We give here just a brief summary of the theory of light scattering from surfmer stabilized particles, pointing for a comprehensive review to ref. 32. We take into account the existence of the surfmer layer of thickness $d \ll R$, where R is the radius of the bare particle. We call n_p, n_l, and n_s the refractive indexes of the bare particle, of the stabilizing layer, and of the solvent respectively. Assuming that the incident field is linearly polarized in the vertical direction and that the scattered field is observed in the horizontal plane, we can write the following expression for the normalized intensity of the light scattered at the same polarization of the incident light by a collection of N diluted particles:

$$I = NV^2\left(1+\frac{d}{R}\right)^6 F^2(x)\left(\overline{n_p^2}-n_s^2\right)^2,$$

where $x = k(R+d)$, $k = (4\pi/\lambda)\sin(\theta/2)$, $a = R/(R+d)$, F is the particle form factor, and

$$\overline{n_p^2} = n_p^2 + \left(n_l^2 - n_p^2\right)\left[1-\frac{R^3F(ax)}{(R+d)^3F(x)}\right]^2.$$

Note that V is here the volume of the bare particle. The minimum of I with respect to n_s corresponds to:

$$n_s' = n_p\left[1+\left(\left(\frac{n_l}{n_p}\right)^2-1\right)\left(1-\frac{R^3F(ax)}{(R+d)^3F(x)}\right)\right]^{1/2}.$$

If we limit our observations to the region $(n_s' - n_s \ll n_s')$, we can approximate $n_s'^2 - n_s^2$ as $2n_s'(n_s' - n_s)$ and write I as a parabolic function of n_s:

$$I = 4NV^2\left(1+\frac{d}{R}\right)^6 F^2(x)n_s'^2\left(n_s'-n_s\right)^2.$$

1.4.4 Density. Particle density was characterized in a temperature-controlled centrifuge equipped with a swinging rotor (Eppendorf 5430 R – Rotor S-24-11-AT). All the measurements were performed at 25 °C.

2 Results and discussion

2.1 Nanoparticle synthesis

RAFT macro-surfmers are macromolecular RAFT agents made up of surfmer units and, for this reason, they preserve their intrinsic ability to act as a surfactant.[33] In the same manner as the classic surfmers they are made up of, they are able to stabilize the NPs and, at the same time, they are covalently linked to the NP surface once used in the emulsion polymerization of hydrophobic monomers, such as fluorinated monomers. However, there are two significant advantages of this method. As opposed to the single surfmers, which are more prone to be buried inside the NPs when they are randomly incorporated into the growing backbone in a classic emulsion polymerization, these species are much bigger. The growth of the NP starts, then, from the RAFT functionalities, producing a well-defined block-copolymer that further improves the NP colloidal stability, as depicted in Fig. 1.

In addition, different charge and functionalities can be easily incorporated on the surface of the NPs by adopting a non-charged PEGylated RAFT macro-surfmer with different length, negatively charged RAFT macro-surfmers such as SPMAK, and/or by carrying out a RAFT copolymerization of a PEGylated monomer and a positively charged monomer, as the ones summarized in Table 1 (further details of the RAFT macro-surfmers synthesis can be found in the ESI†).

Their subsequent use in the *ab initio* RAFT emulsion polymerization of HFIPM can lead to the synthesis of mono-disperse

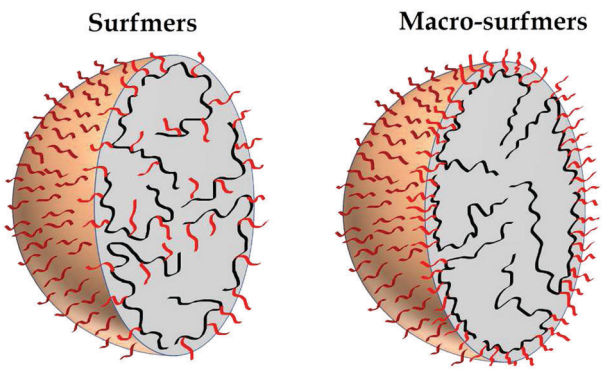

Fig. 1 Difference between NPs made *via* surfmers and RAFT macro-surfmers.

Table 1 Characterization of the RAFT macro-surfmers

Sample (—)	M_n (Da) Theory[a]	GPC[b]	$Đ$ (—)	Conversion (χ)[c] (%)
$(PEGMA950)_{10}$	9779	7755	1.09	89
$(PEGMA2000)_5$	10 279	9274	1.08	83
$(SPMAK)_{10}$	2742	—	—	98
$(MADQUAT)_{10}$	2356	—	—	98.8
$(MADQUAT)_5(PEGMA950)_{10}$	10 817	—	—	97
$(MADQUAT)_{10}(PEGMA950)_{10}$	11 856	—	—	96

[a] Obtained by the equation $M_n = \frac{[M]_0\chi}{[CTA]_0}M_{n,mon} + M_{n,CTA}$. [b] In THF with PS calibration. [c] Conversion of the first three samples was determined by GPC, comparing the area of the RI signal of the monomer at t_0 and at t_{final}.[33] The conversion of the last two samples was obtained by ^{1}H-NMR by comparing the polymer peaks with the double bond peaks.

fluorinated NPs with tunable size just by changing the RAFT macro-surfmer to monomer (S/M) ratio, as visible in Fig. 2, and with different charge, as visible from the ζ-potential values in Table S1 (ESI†).

In all the NPs reported in Fig. 2, the PDI evaluated *via* DLLS (see Table S1, ESI†) is very low – typically less than 5% – except for some NPs synthesized at higher $(PEGMA950)_{10}$/monomer ratios. Interestingly, while $(PEGMA950)_{10}$, $(PEGMA2000)_5$, and $(SPMAK)_{10}$ present a similar ability to stabilize the fluorinated NPs, $(MADQUAT)_{10}(PEGMA950)_{10}$ is less effective and higher S/M are required to obtain monodisperse NPs. It is noteworthy to mention that this can be ascribed to the higher hydrophilicity of this RAFT macro-surfmer compared to the others. To confirm this point we used $(MADQUAT)_{10}$ and $(MADQUAT)_5(PEGMA950)_{10}$ in the NP production. While the first was not able to stabilize the NPs at any S/M ratio reported in Fig. 2, the fluorinated NPs synthesized with $(MADQUAT)_5(PEGMA950)_{10}$ at S/M = 2.5 and 3 are smaller compared to the ones obtained with the $(MADQUAT)_{10}$-$(PEGMA950)_{10}$, as reported in Fig. S4 (ESI†).

Data in Table S1 (ESI†) clearly show that charged NPs have a lower PDI, due to the greater colloidal stability offered by charged surfmers with respect to neutral ones, which can rely

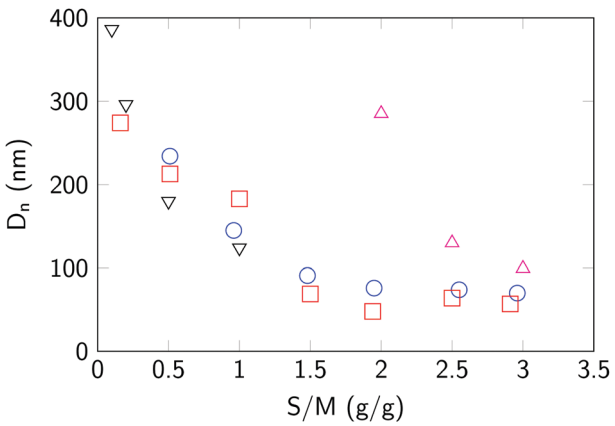

Fig. 2 NP size obtained by varying the RAFT macro-surfmer to monomer ratio. Legend: (○) $(PEGMA2000)_5$; (□) $(PEGMA950)_{10}$; (▽) $(SPMAK)_{10}$; (Δ) $(MADQUAT)_{10}(PEGMA950)_{10}$.

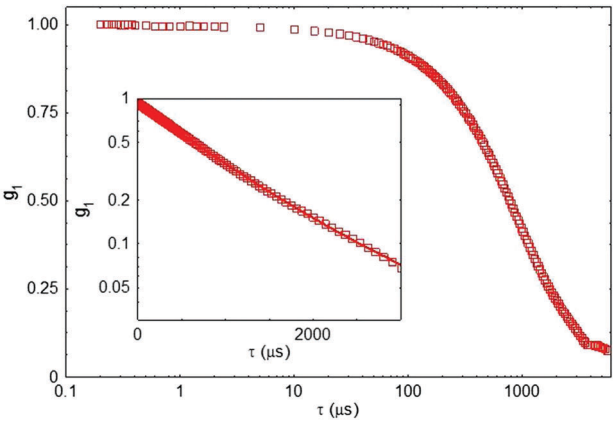

Fig. 3 (Main body) Field correlation function *versus* delay time for NPs of batch A. (Inset) Same curve of the main body in log-lin scale. Continuous line is a third-order cumulant analysis fit.

only on steric stabilization. A typical measure of the field correlation function as obtained by DLLS is visible in Fig. 3 (referring to batch A, see Table 2). In the inset, the logarithm of the curve can be well fitted by a third order polynomial, showing a PDI lower than 3%.

TEM and SEM analysis, as visible in Fig. 4, confirm that the particles are spherical. Moreover, when a droplet of a highly concentrated NPs is dried, it is possible to observe that the sample is sufficiently monodisperse to form close packed crystalline domains. This is indeed consistent with the highly ordered structure of the NPs that are formed by well-defined block-copolymers, as proven from GPC trace of the PEGylated NPs (sample C in Table 2) in Fig. S2 (ESI†) where it is possible to observe a narrow curve, even if a small secondary peak is present at higher elution volume. This latter one can be attributed to un-reacted macro RAFT-surfmer or dead polymer generated during its synthesis in ethanol.[33] In addition, as shown in the ^{1}H-NMR spectrum in Fig. S3 (ESI†), the relative content of the two monomers (HFIPM/PEGMA2000 = 21.6) in the final copolymer is very close to the theoretical one (19.8).

In order to test the properties of this novel fluorinated NPs and the feasibility of their scale up, three NPs have been chosen (see Table 2) and produced in higher amount. Batch A was used to assess PDI and refractive index. Particle density was measured from batch B and the Casimir force was tested by means of fluorescent microscopy, taking advantage of the addition of Rhodamine B to the NPs. The PEG stabilized NPs (batch C) were used to study gelation promoted by variation of aqueous solubility of the stabilizing layer.

2.2 Refractive index

At visual inspection the particle solution is slightly reddish due the presence of the RAFT agent. The light scattering samples were prepared in the following way: the original, concentrated, latex was purified by a dialysis process carried out for several days to remove unreacted species, until a stable low conductivity value is reached. The index of refraction n_s of the solvent used to dilute the particles was varied by mixing water with TDE

Table 2 NPs made by the scale up of the RAFT emulsion polymerization of HFIPM with different RAFT macro-surfmers

Sample	C_{latex}[a] (%)	S/M[b] (g g^{-1})	D_n (nm)	PDI (—)	ζ-Pot (mV)	Dev. ζ-pot (mV)	RAFT macro-surfmer
A	10	0.4	224	0.056	−66	5	$(SPMAK)_{10}$
B	10	1	124	0.057	−47	12	$(SPMAK)_{10}$
C	10	2.5	96	0.107	—	—	$(PEGMA2000)_5$

[a] Monomer to acetic buffer weight ratio. [b] Macro RAFT agent to monomer weight ratio.

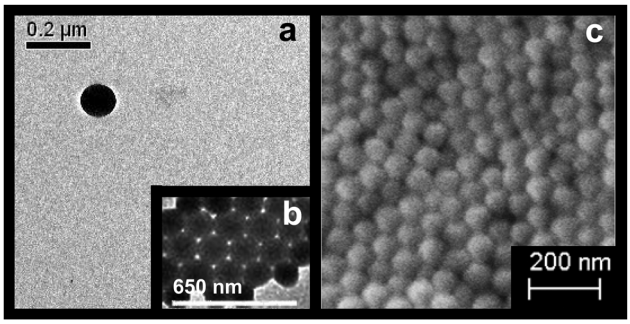

Fig. 4 (a and b) TEM images of negatively charged NPs corresponding to the sample B in Table 2. (c) SEM image of PEGylated NPs corresponding to the sample C in Table 2.

(n_{TDE} = 1.5215). TDE is a nontoxic water soluble embedding medium that was recently proposed for optical microscopy because it is miscible with water at any ratio and thus allows for fine adjustment of the average refractive index of the sample, ranging from water (1.33) to immersion oil (1.52).[34] To exclude any effect of TDE on the NP properties, we checked the experiments by also varying the solvent refractive index with the addition of urea. Unless otherwise stated, the measurements were performed at 25 °C. In the following, we focus on batch A. Similar results can be found for the other NPs batches.

In Fig. 5, we show the scattered intensity I measured as function of the refractive index of the solvent for batch A, containing a particle volume fraction of 0.1%. The values of n are relative to the 589.3 nm Na-D line.

As can be noticed, the intensity reaches a null minimum value, indicating that the particles are amorphous and do not contain crystalline domains as for other fluorinated particles as MFA or PTFE. For this reason, these latter particles cannot be optically matched with their solvent, though the partial optical anisotropy can be exploited to sensitively probe their concentration.[12,13] On the contrary, the NPs we synthesized can be index-matched, reducing the scattered light to negligible values. This fact, combined with the possibility of embedding fluorescent dyes, makes our NPs the ideal candidates for microscopy applications. By fitting the data near the match point with a parabola, the minimum is found at a refractive index of 1.382, comparable to the one found for analogous NPs.[27] The refractive index of the particles is similar for every batch we synthesized, indicating that the surfmer layer does not significantly affect the refractive index of the particles. It is worth to mention that, as shown in ref. 12, the position of the minimum can depend in principle on the scattering angle and this effect can be exploited to obtain further information on the surfmer layer refractive index and thickness. This study is beyond the scope of the present work and it is let for future investigation.

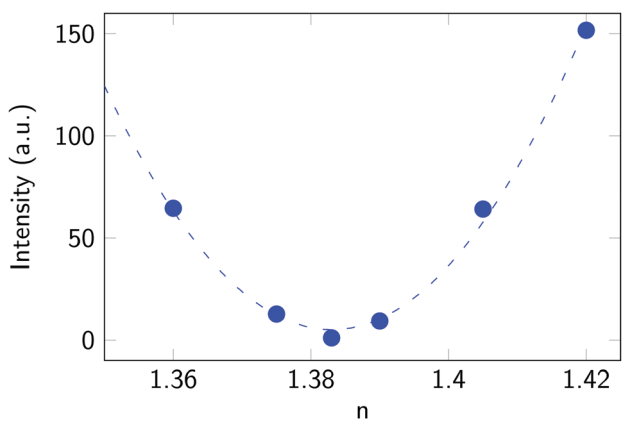

Fig. 5 Intensity for particles of batch A *versus* solvent refractive index.

2.3 Particle density

In order to obtain the density of the NPs, we performed centrifugation against solvents with different density, taking advantage of the great stability of our NPs in high ionic strength solutions by dispersing them in mixtures of water and SPT. SPT is a highly soluble inorganic salt that, when dissolved in water, can be used to replace the toxic and possible carcinogenic organic liquids, such as bromoform and tetrabromoethane, traditionally used in gravity separation processes. Some of the advantages of using SPT are simple handling, low flammability, and no corrosiveness. More important, the density of SPT–water mixture can be adjusted from 1.0 g cm^{-3} to 3.1 g cm^{-3} and results in an aqueous, colorless, and transparent neutral solution. At room temperature, the viscosity of the mixture increases with the concentration of the SPT but, for densities below 2.0 g cm^{-3}, it remains less than 4 times the viscosity of pure water.

In Fig. 6 we show the result of the centrifugation of Rhodamine-labelled NPs of batch B at 16 000*g* for 2 hours at different solvent densities, ρ. For $\rho < 1.490$ g cm^{-3}, a cake at the bottom of the microtube formed, as indicated by the presence of a darker band. On the contrary, for $\rho > 1.510$ g cm^{-3}, the particles cream to the top of the centrifuge microtube, showing the formation of a clear subnatant. For $\rho \sim 1.490$ g cm^{-3} a very slow sedimentation is barely discernible. We followed the evolution of this sample for a longer period and from the motion of the sedimentation front with time it was possible to extract a density of the particle equal to $\rho_P \sim 1.492$ g cm^{-3}.

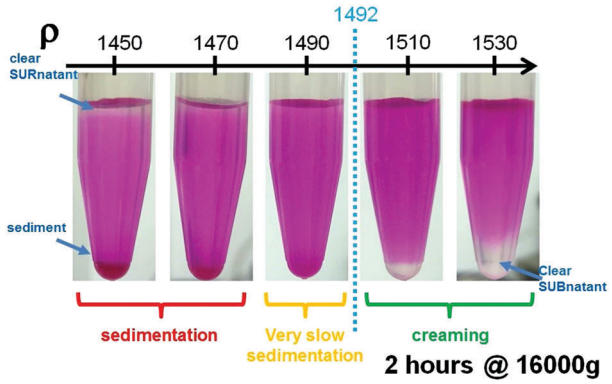

Fig. 6 Sedimentation of NPs of batch B at different solvent density.

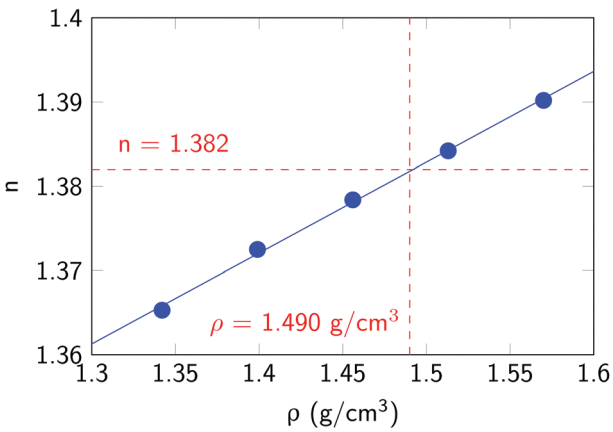

Fig. 7 Refractive index of SPT/water mixtures at different densities.

By serendipity, at this density value the refractive index of an aqueous solution of SPT is $n_s \sim 1.382 \approx n_p$, as shown in Fig. 7. In this view, considering that (i) the particles can be simultaneously density and optically matched without effort, (ii) that the amount of SPT added to the solvent is sufficient to completely screen electrostatic interactions,‡ and (iii) that the particles do not swell in water, our fluorinated NPs can be regarded as a good candidate for a hard spheres model system that can overcome some of the problems pointed out in ref. 35. To quantify how precisely our NPs behave as hard sphere further investigations, as ones proposed in ref. 13, will be performed in the future.

To show the potential of our NPs as aqueous colloidal model systems, in the following we briefly present two uses of our NPs suspensions to study gelation.

2.4 Case study I: gelation promoted by critical Casimir forces

In the last years, different works have demonstrated the active assembly control of colloidal phases using critical Casimir forces (CCF).[36–39] Close to the critical point of a binary liquid, concentration fluctuations become long-ranged and the confinement of these long-range fluctuations gives rise to critical Casimir interactions, in analogy to the quantum mechanical Casimir effect.[40] In a colloidal solution made of particles dispersed in such a binary liquid, the solvent fluctuations confined between the particles surfaces lead to an effective attraction that can be tuned by adjusting the temperature. In this context, the most used binary mixture consists of 3-methylpyridine (3MP) and water (in some cases heavy water was added to density match the system) which, despite its common use, is toxic and – as other pyridine derivatives – an environmental contaminant. The use of this compound for experiments on board of the International Space Station (ISS) requires at least three levels of containment between the sample and the astronauts. One of the authors is currently developing a new modular light scattering apparatus, called "COLIS", that will be installed on board of the ISS. By design, to reduce the cost and simplify the change of samples, in this new setup there will be only two level of confinement. For this reason, 3MP cannot be used, although the scientific community have shown a great interest in studying CCF in microgravity conditions. In literature, binary mixtures of non-ionic surfactant/water, that do not present problem of toxicity, have been used in the context of CCF.[38,41,42] A drawback of the use of surfactants is that micelles themselves can induce unwanted aggregation by depletion forces already at room temperature. To avoid these difficulties, we have tested the use of 1-propoxy-2-propanol (1P2P) as an alternative to 3MP. As is well-known, glycol ethers based solvents have been used in industry since the 1970s and could be found in various commercial products. For this reason, the majority of glycol ethers currently commercially available have been tested for their toxic properties, showing some of them are genotoxic. As a consequence, they are progressively being phased-out from the market and substituted in the formulation of domestic products by glycol ethers of the propylenic series, which are much less toxic.[43] Between the family of propylene glycol alkyl ethers solvents, we chose 1P2P because it shows a de-mixing curve with water, with a critical concentration $c_c \simeq 0.4$ w/w and a critical temperature $T_c \simeq 32$ °C, not too far from room temperature (see Fig. 8).

As known, the dispersion of NPs in this binary mixture for a 1P2P fraction higher than critical one is not easy, due to reduced polarizability of the solvent, and we are not able to successfully disperse PEGylated NPs in 1P2P/water mixtures with $c \geq c_c$. On the contrary, we have verified that negatively charged NPs are stable in 1P2P/water mixtures. As with 3PM mixtures, we can induce critical Casimir interactions by approaching the phase-separation temperature T_c of the binary solvent, and we can easily tune the interactions changing the temperature or the amount of added NaCl.

As can be noticed in Fig. 8, the aggregation of NPs is not symmetric with respect to the critical composition, but it happens at lower temperature for mixture richer of 1P2P. In addition, while for unscreened electrostatic interactions NPs aggregation takes place very close to the de-mixing curve,

‡ To index – and density match our NPs is necessary to add around 200 mM of SPT, a multivalent salt. At this ionic strength the Debye length is less than 1 nm and SPT alone is sufficient to screen the electrostatic interactions. Of course more common salts can be used: in fact our NPs are stable in more than 1 M of NaCl, where the Debye length is less than 0.3 nm and electrostatic effect are negligible.

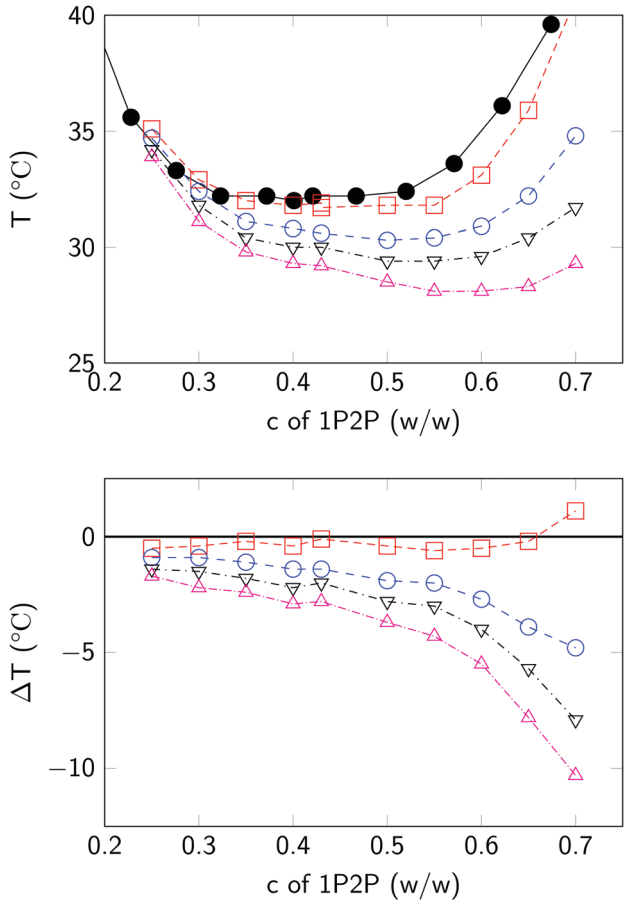

Fig. 8 (upper panel) Minimum amount of 1P2P concentration needed to induce phase separation for negatively charged NPs of radius 124 nm, in the presence of different amount of NaCl, at a particle volume fraction ϕ = 0.03. (lower panel) Same curves of left panel where, for each 1P2P concentration, we have subtracted the de-mixing temperature at that composition. Legend: (●) Consolution curve of the 1P2P/water mixture; (□) no added salt; (○) 1 mM NaCl; (▽) 2 mM NaCl; (Δ) 3 mM NaCl.

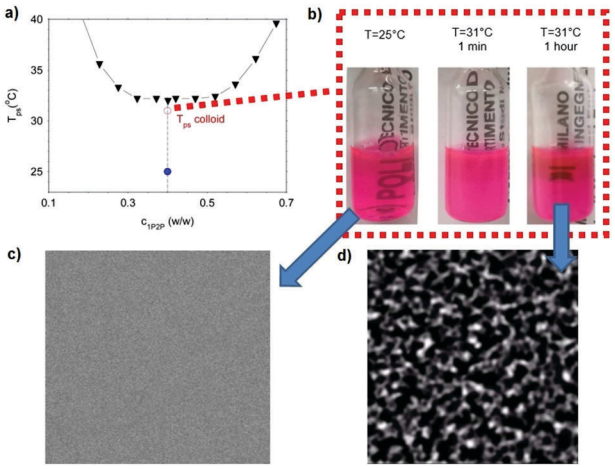

Fig. 9 (a) Location in the 1P2P/water phase diagram of the samples imaged in panel (c) and (d). (b) Gelation induced by a T jump. For T = 25 °C the colloidal solution is stable and transparent (○ in panel (a)). For T = 31 °C (●) the sample forms a gel phase that eventually collapse to the bottom of the cell. (c) Fluorescence image of the sample a T = 25 °C. (d) Fluorescence image of the same sample at T = 31 °C. Images of panel (c) and (d) have a field of view of 200 μm × 200 μm.

increasing the ionic strength we have aggregation at more than 8 °C from the binodal curve. These results are consistent with previous experimental results for 3MP/water mixtures.[39] We note that at NaCl concentrations higher than 4 mM we start to have particle aggregation at room temperature.

In Fig. 9 we show an example of gel formation promoted by CCF. At T = 25 °C, the sample is stable and transparent at a visual inspection (see panel (b)). When we increase the temperature of the system to T = 31 °C, the sample suddenly becomes turbid and – after a transient period – starts to settle with a sedimentation velocity orders of magnitude faster than for stable solution. After 1 h the concentrated phase accumulates at the bottom of the cell. This phase coexists with a very diluted one that floats on top, as witnessed by the light pink color of the surnatant showed in panel (b). Thanks to the fluorescence of NPs, the gelation mechanism can be followed at the microscale using an optical microscope equipped with fluorescence detection (details of the setup and the correction for bleaching can be found in the ESI†). The bottom panels of Fig. 9 show that, while for the stable solution particles are too small to be resolved and a homogenous fluorescence signal is present, for the gelated sample it is possible to clearly resolve the strands that form the gel network. In the ESI,† the evolution of the gel with strands forming and breaking can be appreciated in real time from the uploaded video.

Once the temperature is reduced back to 25 °C, the gel disappears and the NPs can be easily dispersed again by a gentle shaking. This result confirms the reversible nature of the aggregation mechanism.

The preliminary findings we describe demonstrate that our charged fluorinated NPs and 1P2P/water mixtures can profitably be used as a model system to study CCF in concentrated samples. In addition, the capability to precisely tune the surface charge by controlling the type of surfmers can be exploited to investigate the subtle interplay between critical phenomena and electrostatics that theories[44] and experiment[45] have recently pointed out.

2.5 Case study II: gelation promoted by variation of aqueous solubility of PEG

As shown in the past,[27] the interactions among PEG-grafted colloids follow qualitatively the aqueous solubility of PEG. The NP potential can be easily tuned from repulsive to attractive, under good and marginal solvent conditions respectively, in a fully reversible way. We verify these properties on our NPs stabilized by $(PEGMA2000)_5$ RAFT macro-surfmer (batch C) at fixed volume fraction ϕ = 0.08. In this case the length of the PEG chain is sufficiently long such that when we increase the temperature of the sample up to 60 °C there is no evidence of particle aggregation. On the contrary, if we add 600 mM of ammonium sulfate, which is known to cause phase separation in PEG solutions, at $T > T_{gel}$ = 42 °C the particles rapidly aggregate to form a gel structure that, after a transient time, settles under its own weight. When the temperature is reduced

below 42 °C the gel easily re-melts. The gel compressive modulus is also temperature dependent, as witnessed by the fact that gels formed at higher temperature compress less than ones solidified at lower T.

We take advantage of the low turbidity of our samples to study the melting of these gels using Digital Fourier Imaging (DFI),[46–48] a novel class of optical correlation techniques combining the power of scattering and microscopy. A complete review of DFI can be found in ref. 46. Recently DFI has allowed to pick out novel useful evidences concerning the restructuring processes taking place in colloidal gels.[47,48] The key idea behind DFI is to collect the light scattered by the sample in "near field" (NF), which more technically means on a plane lying within the so called "deep Fresnel" diffraction region. In the general case, the power spectrum of the intensity on a NF plane is directly related to the structure factor of a suspension. Then, a simple DFI scattering experiment just consists of sending a spatial coherent light beam on the sample and collecting the optical signal with a camera placed along the optical axis at a short distance z from the sample. The intensity pattern on the detection plane shows a time-fluctuating speckle pattern, whose amplitude is modulated by the transmitted field. The fluctuation in time of each single speckle is related to the microscopic dynamics of the sample as a superposition of the decay modes for all the detected scattering-vectors q. While these decay modes can be set apart by Fourier Analysis, yielding the correlation function at each q, a straightforward impression of how fast is the local microscopic dynamics in the sample at time t is provided by an activity map, obtained from the standard deviation over small averaging blocks of the intensity difference between two images.

In the following case study we will focus on a sample at $\phi = 0.08$, where gelation is promoted by increasing, at time $t = 0$, the temperature to $T = 45$ °C. After 5 minutes the temperature was decreased to $T = 41$ °C $< T_{gel}$ with a cooling rate of around 0.1 °C s^{-1}. The local dynamics during gel melting can be better quantified by plotting the activity maps at different values of t, obtained by evaluating in a small circular block around each position in the gel the standard deviation $\sigma(\mathbf{r},t)$ of the difference signal between two images acquired at t and $t + \Delta t$, with $\Delta t = 2.5$ s, which increases the more the two speckle fields become uncorrelated. In Fig. 10 the activity maps are overlaid on images of the gel taken at distinct stages of the gel melting: the more a region is reddish, the faster its dynamics. Panel (a) refers to the gel at $t = 5$ min, before the start of the cooling process, when $T = 45$ °C. The speckle pattern is well visible and the dynamics are arrested. Panel (b) corresponds to $t = 5$ min 30 s, where the temperature is slightly higher than T_{gel}. A region of faster dynamics is clearly visible on the right of the image, while the rest of the sample experiences only a limited change in configuration. This is a weak point of the gel network and a discrete strand dissociation event occurs. The number of these events increases approaching the T_{gel} until the dynamics of the whole gel network is activated when $T < T_{gel}$ (panel (c)). Eventually the gel completely melts and the speckle pattern disappears, as shown in the last panel. The fact that in this gel the stress release associated with a strand dissociation is localized, is in contrast with experimental findings in strong gels, where these events extend over strikingly large length scales – comparable to the system size – suggesting that any local rearrangement must propagate very far throughout the network.[48–50]

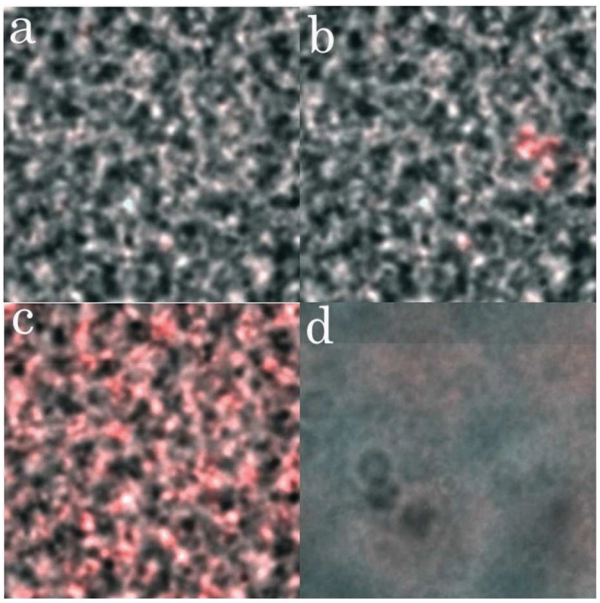

Fig. 10 NF images of the gel described in the text, overlaid with "Activity maps" at four different stages of gel melting. Red color indicates fast rearrangement dynamics. The field of view is 200 μm × 200 μm.

The use of our NPs in this context can help to elucidate mechanical stress transmission in different typologies of colloidal gels.

3 Conclusion

Fluorinated NPs have been synthesized with different concentration, dimension and surface charge adopting RAFT macro-surfmers made up of amphiphilic monomers. Different RAFT macro-surfmers based on poly(ethylene glycol) methyl ether methacrylate (PEGMA950 and PEGMA2000), [2-(methacryloyloxy)ethyl] trimethylammonium chloride (MADQUAT) and 3-sulfopropyl methacrylate potassium salt (SPMAK) have been obtained. Then, they have been used in the *ab initio* RAFT emulsion polymerization of a partially fluorinated methacrylate (HFIPM) to produce NPs with a wide range of size and surface charge and optimal characteristics in terms of stability and PDI without the use of toxic fluorinated surfactants.

The adoption of these novel surface active species allows for the functionalization of the NP surface and, moreover, to improve the colloidal stability. Indeed, the bigger and more ordered RAFT macro-surfmers are less prone to be buried inside the NPs core compared to a single surfmer that, otherwise, can be easily incorporated into the highly hydrophobic backbone and dragged inside.

We have demonstrated that the addition to the solvent of sodium polytungstate, an inorganic salt widely used as a heavy

liquid for gravity separation and density gradient centrifugation, can simultaneously match the optical index and the density of the NPs. Combined with the possibly to control the charge of the stabilizer and the particle interactions, these dispersions can be used as model systems in colloidal science, with the great advantage that fluorinated NPs do not swell in water, contrary to the popular hard spheres model system of PMMA/*cis*-decalin/bromocyclohexane, leading to a precise determination of particles radii and of the solid volume fraction.

Conflicts of interest

There are no conflicts to declare.

Acknowledgements

We thank R. Piazza for useful discussions, J. G. Rosenboom (ETH) for the GPC data of the PEGylated NPs in HFIP, and A. Klaue (ETH) for SEM images. We acknowledge funding by the Italian Ministry of Education and Research (''Futuro in Ricerca'' Project Anisoft/RBFR125H0M and PRIN 2012 ''Oltre Archimede: nuovi principi e tecniche per la sedimentazione e la centrifugazione di miscele colloidali e fluidi biologici''). C. T. Canova acknowledges funding by the Rocca Research Grants for MIT graduate student.

References

1 M. P. Krafft, *Adv. Drug Delivery Rev.*, 2001, **47**, 209–228.
2 Y.-C. Chen, W. Yang, J.-G. Qian, D. Xiao Han, X.-Q. Wang and L.-Q. Zhu, 2012 International Conference on Biomedical Engineering and Biotechnology, IEEE, Piscataway, 2012.
3 X. Li, F. Qin, L. Yang, L. Mo, L. Li and L. Hou, *Int. J. Nanomed.*, 2014, **9**, 3971–3985.
4 G. Liu, W. Fan, L. Li, P. K. Chu, K. W. K. Yeung, S. Wu and Z. Xu, *J. Fluorine Chem.*, 2012, **141**, 21–28.
5 J. G. Riess, *J. Fluorine Chem.*, 2002, **114**, 119–126.
6 J. Raphael and C. Lynch III, *Can. J. Anaesth.*, 2009, **56**, 91–95.
7 J. P. Fast, M. G. Perkins, R. A. Pearce, R. M. Waters and S. Mecozzi, *Anesthesiology*, 2008, **109**, 651–656.
8 P. I. R. Muraro, A. G. O. de Freitas, S. G. Trindade, F. C. Giacomelli, J.-J. Bonvent, V. Schmidt, F. P. dos Santos and C. Giacomelli, *J. Fluorine Chem.*, 2014, **168**, 251–259.
9 L. Nurmi, H. Peng, J. Seppälä, D. M. Haddleton, I. Blakey and A. K. Whittaker, *Polym. Chem.*, 2010, **1**, 1039–1047.
10 N. R. B. Boase, I. Blakey and K. J. Thurecht, *Polym. Chem.*, 2012, **3**, 1384–1389.
11 P. N. Pusey and W. van Megen, *Nature*, 1986, **320**, 340–342.
12 V. Degiorgio, R. Piazza and T. Bellini, *Adv. Colloid Interface Sci.*, 1994, **48**, 61–91.
13 S. Buzzaccaro, R. Rusconi and R. Piazza, *Phys. Rev. Lett.*, 2007, **99**, 098301.
14 G. Brambilla, S. Buzzaccaro, R. Piazza, L. Berthier and L. Cipelletti, *Phys. Rev. Lett.*, 2011, **106**, 118302.
15 M. Jiang, Z. Zheng, X. Ding, X. Cheng and Y. Peng, *Colloid Polym. Sci.*, 2007, **285**, 1049–1054.
16 T. Cserháti, E. Forgács and G. Oros, *Environ. Int.*, 2002, **28**, 337–348.
17 G.-G. Ying, *Environ. Int.*, 2006, **32**, 417–431.
18 M. M. Schultz, D. F. Barofsky and J. A. Field, *J. Environ. Eng. Sci.*, 2004, **20**, 487–501.
19 F. M. Hekster, R. W. P. M. Laane and P. de Voogt, *Rev. Environ. Contam. Toxicol.*, 2003, **179**, 99–121.
20 H.-J. Lehmler, *Chemosphere*, 2005, **58**, 1471–1496.
21 J. M. Asua and H. A. S. Schoonbrood, *Acta Polym.*, 1998, **49**, 671–686.
22 J. Wang, X.-R. Zeng and H.-Q. Li, *J. Coat. Technol. Res.*, 2010, **7**, 469–476.
23 X. Xiao and Y. Wang, *Colloids Surf., A*, 2009, **348**, 151–156.
24 G. Xu, L. Deng, X. Wen, P. Pi, D. Zheng, J. Cheng and Z. Yang, *J. Coat. Technol. Res.*, 2011, **8**, 401–407.
25 M. Wiemann, R. Schneider and E. Bartsch, *Z. Phys. Chem.*, 2012, **226**, 761–778.
26 D. Burger, J. Gisin and E. Bartsch, *Colloids Surf., A*, 2014, **442**, 123–131.
27 J. Ulama, M. Z. Oskolkova and J. Bergenholtz, *J. Phys. Chem. B*, 2014, **118**, 2582–2588.
28 C. J. Ferguson, R. J. Hughes, D. Nguyen, B. T. T. Pham, R. G. Gilbert, A. K. Serelis, C. H. Such and B. S. Hawkett, *Macromolecules*, 2005, **38**, 2191–2204.
29 J. Chiefari, Y. K. B. Chong, F. Ercole, J. Krstina, J. Jeffery, T. P. T. Le, R. T. A. Mayadunne, G. F. Meijs, C. L. Moad, G. Moad, E. Rizzardo and S. H. Thang, *Macromolecules*, 1998, **31**, 5559–5562.
30 S. W. Prescott, M. J. Ballard, E. Rizzardo and R. G. Gilbert, *Aust. J. Chem.*, 2002, **55**, 415–424.
31 J. Zhou, L. Zhang and J. Ma, *Chem. Eng. J.*, 2013, **223**, 8–17.
32 M. Dossi, R. Ferrari, L. Dragoni, C. Martignoni, P. Gaetani, M. D'Incalci, M. Morbidelli and D. Moscatelli, *Macromol. Mater. Eng.*, 2013, **298**, 771–778.
33 U. C. Palmiero, A. Agostini, S. Gatti, M. Sponchioni, V. Valenti, L. Brunel and D. Moscatelli, *Macromolecules*, 2016, **49**, 8387–8396.
34 T. Staudt, M. C. Lang, R. Medda, J. Engelhardt and S. W. Hell, *Microsc. Res. Tech.*, 2007, **70**, 1–9.
35 C. P. Royall, W. C. K. Poon and E. R. Weeks, *Soft Matter*, 2013, **9**, 17–27.
36 C. Hertlein, L. Helden, A. Gambassi, S. Dietrich and C. Bechinger, *Nature*, 2008, **451**, 172–175.
37 V. D. Nguyen, S. Faber, Z. Hu, G. H. Wegdam and P. Schall, *Nat. Commun.*, 2013, **4**, 1584.
38 S. Buzzaccaro, J. Colombo, A. Parola and R. Piazza, *Phys. Rev. Lett.*, 2010, **105**, 198301.
39 D. Bonn, J. Otwinowski, S. Sacanna, H. Guo, G. Wegdam and P. Schall, *Phys. Rev. Lett.*, 2009, **103**, 156101.
40 M. E. Fisher and P.-G. de Gennes, *C. R. Seances Acad. Sci., Ser. B*, 1978, **287**, 207–209.
41 S. Buzzaccaro, *Nuovo Cimento*, 2011, **34**, 109–118.
42 R. Piazza, S. Buzzaccaro, A. Parola and J. Colombo, *J. Phys.: Condens. Matter*, 2011, **28**, 194114.

43 P. Bauduin, Doctoral dissertation, University of Regensburg, 2005.
44 U. Nellen, J. Dietrich, L. Helden, S. Chodankar, K. Nygård, J. F. van der Veen and C. Bechinger, *Soft Matter*, 2011, **7**, 5360–5364.
45 F. Pousaneh, A. Ciach and A. Maciołek, *Soft Matter*, 2012, **8**, 7567–7581.
46 R. Cerbino and V. Trappe, *Phys. Rev. Lett.*, 2008, **100**, 188102.
47 F. Giavazzi and R. Cerbino, *J. Opt.*, 2014, **16**, 083001.
48 S. Buzzaccaro, M. D. Alaimo, E. Secchi and R. Piazza, *J. Phys.: Condens. Matter*, 2015, **27**, 194120.
49 E. Secchi, T. Roversi, S. Buzzaccaro, L. Piazza and R. Piazza, *Soft Matter*, 2013, **9**, 3931–3944.
50 A. Duri, D. A. Sessoms, V. Trappe and L. Cipelletti, *Phys. Rev. Lett.*, 2009, **102**, 085702.

Supporting Information

Use of RAFT Macro-Surfmers for the Synthesis of Transparent Aqueous Colloids with Tunable Interactions

Synthesis of RAFT Macro-Surfmers

The molecular weight obtained by GPC is not accurate since PS calibration was used but confirms the trend of the control of the polymerization.

The produced RAFT Macro-Surfmers were also analyzed by ^{1}H-NMR and the results are shown in Figure 2, confirming the purity of the products. Due to the high reactivity of the charged monomers – MADQUAT and SPMAK – in water, the presence of the peaks relative to the double bond is almost imperceptible and the conversion obtained by comparing the monomer and polymer peaks is very high, 96% and 98% respectively. For the PEG based RAFT Macro-Surfmers the conversion is lower (89%). In order to verify the efficacy of the purification step the ^{1}H-NMR of the positively charged RAFT Macro-Surfmer (2b) was analyzed before the dialysis step, whereas the negatively charged one (2c) was analyzed after and as expected the peak of the sodium acetate (NaOAc) relative to the acetic buffer was respectively present and not present.

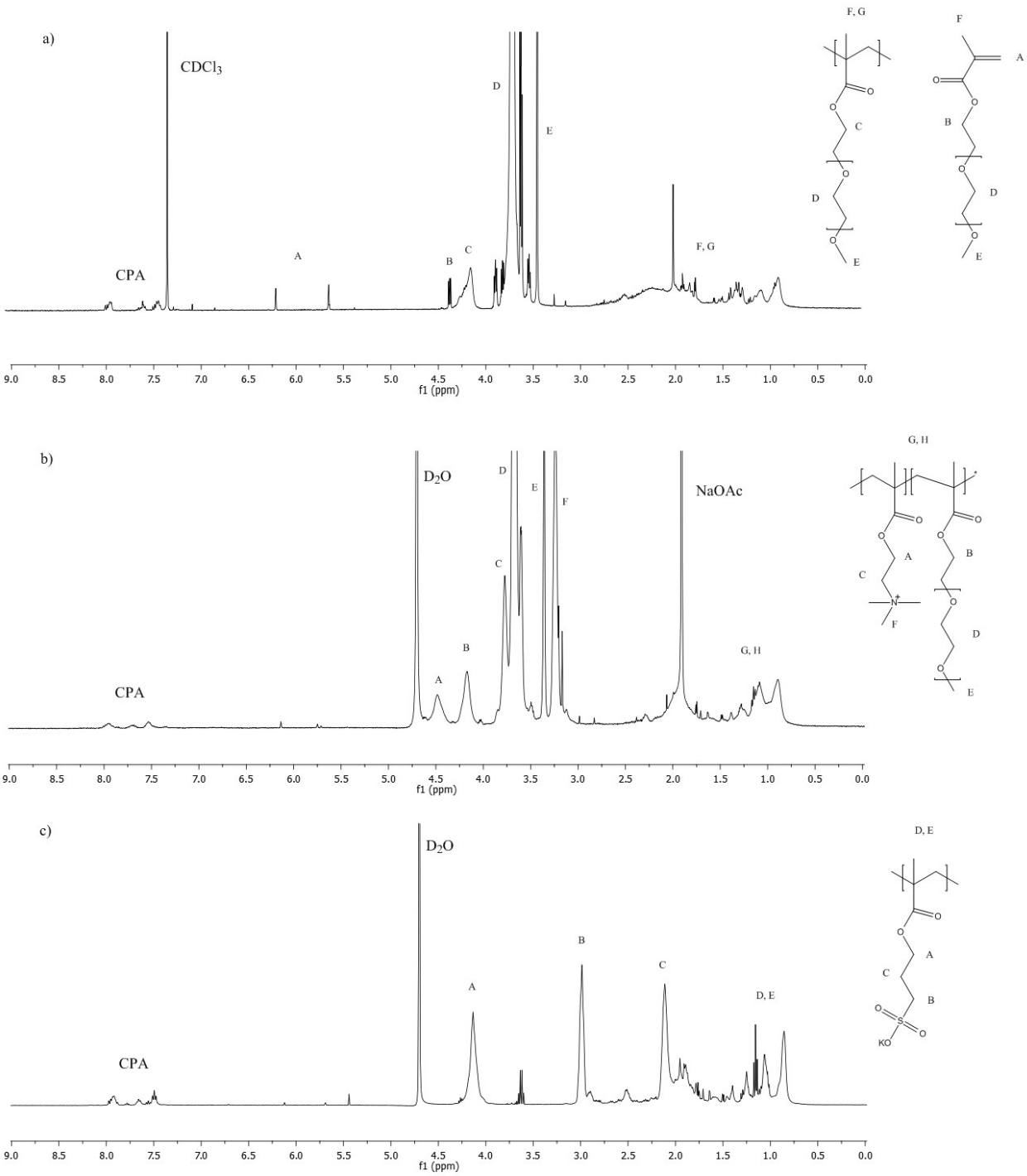

Figure S1. ^{1}H-NMR spectra of the RAFT Macro-Surfmers: a) $(PEGMA950)_{10}$; b) $(MADQUAT)_{10}(PEGMA950)_{10}$; c) $(SPMAK)_{10}$

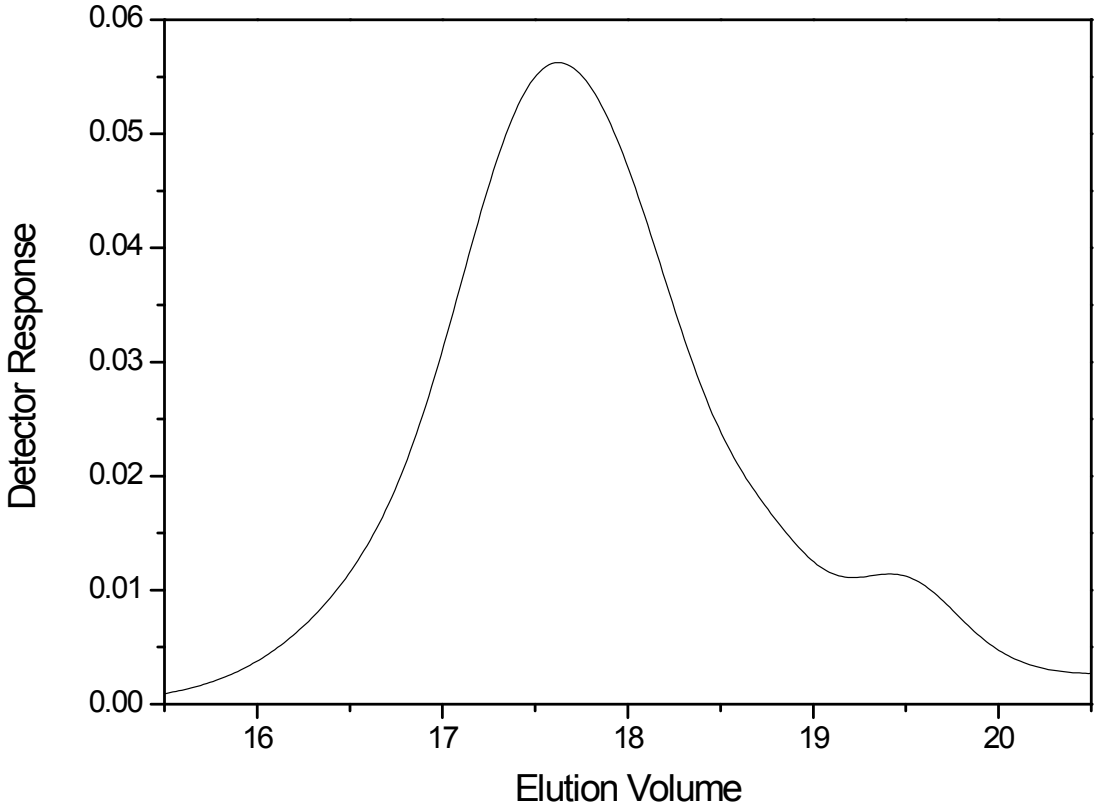

Figure S2: GPC trace of the PEGylated block-copolymer that forms the neutral fluorinated NPs reported as sample C in Table 2.

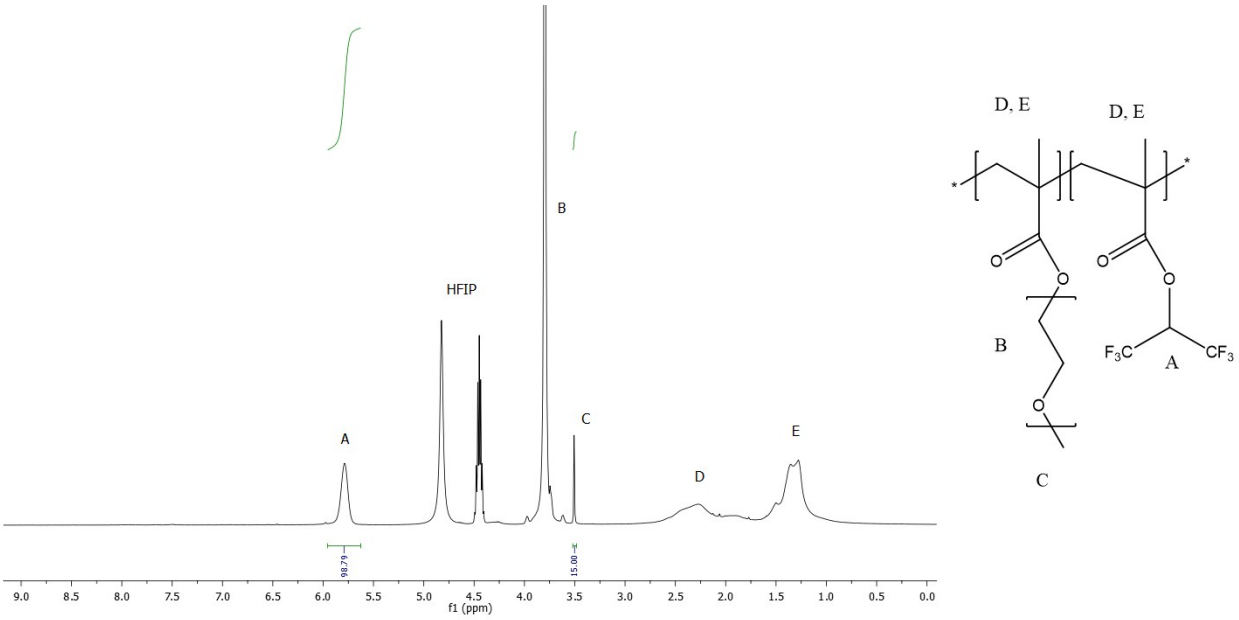

Figure S3: ^{1}H-NMR spectrum of the PEGylated block-copolymer that forms the neutral fluorinated NPs reported as sample C in Table 2. The relative content of the two monomers is evaluated as HFIPM/PEGMA2000 = A/3C

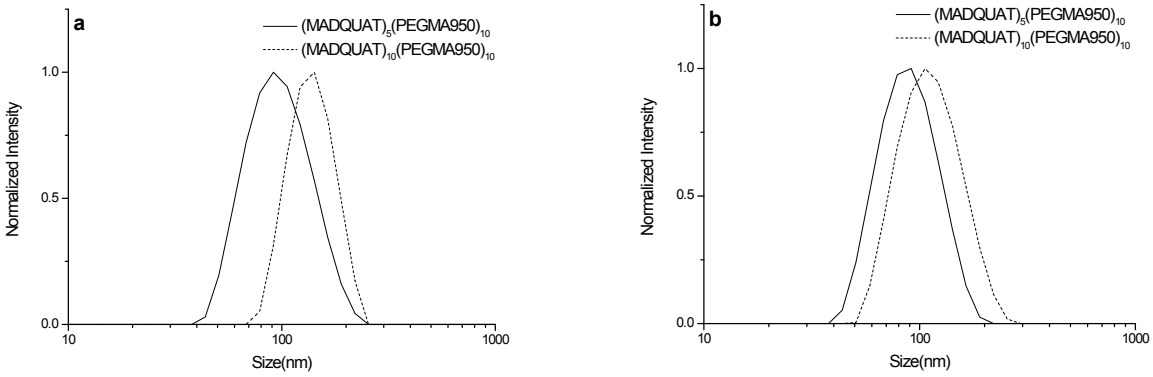

Figure S4: (a) NP size distribution of fluorinated NPs made with $(MADQUAT)_5(PEGMA950)_{10}$ and $(MADQUAT)_{10}(PEGMA950)_{10}$ at S/M = 2.5; (a) NP size distribution of fluorinated NPs made with $(MADQUAT)_5(PEGMA950)_{10}$ and $(MADQUAT)_{10}(PEGMA950)_{10}$ at S/M = 3.

Synthesis of Fluorinated NPs

Table S1. NPs made by RAFT emulsion polymerization of HFIPM with different RAFT Macro-Surfmers

Sample [#]	Clatex [a] [%]	S/M [b] [g/g]	Dn [nm]	PDI [-]	ζ-pot [mV]	Dev. ζ-pot [mV]	RAFT Macro-Surfmers
NEU1	2.9	0.51	234	0.034	-	-	$(PEGMA2000)_5$
NEU2	3.9	0.96	145	0.014	-	-	$(PEGMA2000)_5$
NEU3	4.8	1.48	91	0.083	-	-	$(PEGMA2000)_5$
NEU4	5.7	1.95	76	0.067	-	-	$(PEGMA2000)_5$
NEU5	6.5	2.55	74	0.05	-	-	$(PEGMA2000)_5$
NEU6	7.4	2.96	70	0.097	-	-	$(PEGMA2000)_5$
NEU7	2-3	0.16	320	0.248	-	-	$(PEGMA950)_{10}$
NEU8	2.9	0,51	267	0.447	-	-	$(PEGMA950)_{10}$
NEU9	3.9	0.97	142	0.383	-	-	$(PEGMA950)_{10}$
NEU10	4.8	1.51	72	0.085	-	-	$(PEGMA950)_{10}$
NEU10	5.7	1.96	83	0.042	-	-	$(PEGMA950)_{10}$
NEU10	6.6	2.45	71	0.061	-	-	$(PEGMA950)_{10}$
NEU10	7.4	3	63	0.094	-	-	$(PEGMA950)_{10}$
NEG1	2.2	0.1	386	0.156	-55	9	$(SPMAK)_{10}$
NEG2	2.4	0.2	296	0.011	-60	11	$(SPMAK)_{10}$
NEG3	2.9	0.5	180	0.022	-43	15	$(SPMAK)_{10}$
NEG4	2	1	116	0.058	-47	5	$(SPMAK)_{10}$
POS1	5.66	2	285.2	0.108	12.4	7.73	$(MADQUAT)_{10}(PEGMA950)_{10}$
POS2	6.54	2.5	130.1	0.018	25.1	8.14	$(MADQUAT)_{10}(PEGMA950)_{10}$
POS3	7.41	3	99.46	0.041	22.2	5.7	$(MADQUAT)_{10}(PEGMA950)_{10}$

a) monomer to acetic buffer weight ratio; b) RAFT Macro-Surfmers to monomer weight ratio.

Optical setup for Fluorescence Imaging and DDM

Our setup consists of a standard Olympus IX70 microscope equipped with long working distance objectives (50X, N.A. 0.55) and a Mercury Lamp (U-RLF-T) for fluorescence imaging. Fluorescent images are acquired with an industrial camera (Prosilica GX1050, Allied Vision, 12 bit, 1024 x 1024). The bleaching of the sample was compensated by software using the "*Bleach Correction*" plugin of ImageJ, using the "*Simple Ratio*" correction method. The "*Integral Image Filters-> Normalize Local Contrast*" was used to enhance the contrast and compensate for not uniform illumination.

In the case of DDM, we used the same optical setup, but in this case the microscope was used in Bright Field configuration. The typical exposure time is of few milliseconds and the condenser numerical aperture is set between 0.10<N.A.<0.15. The microscope capillary is mounted on a custom made cell holder which temperature is fixed by a Peltier module controlled through a PID temperature controller (LFI 3751 Wavelength Electronics).